

# Separation of foregrounds from cosmic microwave background observations with the MAP satellite

A.W. Jones, M.P. Hobson and A.N. Lasenby

*Cavendish Astrophysics, Cavendish Laboratory, Madingley Road, Cambridge CB3 0HE, UK*

Accepted ????. Received ????. in original form 13 December 2018

## ABSTRACT

Simulated observations of a  $10^\circ \times 10^\circ$  field by the Microwave Anisotropy Probe (MAP) are analysed in order to separate cosmic microwave background (CMB) emission from foreground contaminants and instrumental noise and thereby determine how accurately the CMB emission can be recovered. The simulations include emission from the CMB, the kinetic and thermal Sunyaev-Zel'dovich (SZ) effects from galaxy clusters, as well as Galactic dust, free-free and synchrotron. We find that, even in the presence of these contaminating foregrounds, the CMB map is reconstructed with an rms accuracy of about  $20 \mu\text{K}$  per  $12.6$  arcmin pixel, which represents a substantial improvement as compared to the individual temperature sensitivities of the raw data channels. We also find, for the single  $10^\circ \times 10^\circ$  field, that the CMB power spectrum is accurately recovered for  $\ell \lesssim 600$ .

**Key words:** methods: data analysis – techniques: image processing – cosmic microwave background.

## 1 INTRODUCTION

The NASA MAP satellite is due to be launched in 2000 and aims to make high-resolution, low-noise maps of the whole sky at several observing frequencies. The main goal of the mission is to use this multi-frequency data to produce an all-sky map of fluctuations in the cosmic microwave background (CMB). As with any CMB experiment, however, MAP is also sensitive to emission from several foreground components. The main contaminants are expected to be Galactic dust, free-free and synchrotron emission, the kinetic and thermal Sunyaev-Zel'dovich (SZ) effect from galaxy clusters, and extra-galactic point sources. In order to obtain a map of the CMB fluctuations alone, it is therefore necessary to separate the emission from these various components.

The contamination due to extra-galactic point sources is expected to be mainly from radio-loud AGNs, including flat spectrum radio-galaxies and QSOs, blazars and possibly some inverted spectrum radiosources. Since the frequency spectra of many of these extra-galactic objects are, in general, rather complicated, any extrapolation of their emission over a wide frequency range must be performed with caution. For MAP observations it is possible that a significant fraction of point sources may be identified and removed using the satellite observations themselves, together perhaps with pre-existing surveys. Moreover, by including the point source predictions of Toffolatti et al. (1998) into simulated Planck Surveyor observations, Hobson et al. (1998b) find, using a maximum-entropy algorithm, that the quality of the component separation is relatively insensitive to the presence of the point sources. Therefore, the effects of point sources will be ignored in this paper.

Aside from extra-galactic point sources, the other physical

components mentioned above have reasonably well defined spectral characteristics, and we may use this information, together with multi-frequency observations, to distinguish between the various foregrounds. In this paper, we perform a separation of the different components, in order to determine the accuracy to which the MAP satellite can recover the CMB emission in the presence of contaminating foreground emission. The separation is carried out using the Fourier space maximum-entropy method (MEM) developed by Hobson et al. (1998) (hereafter HJLB98), which in the absence of non-Gaussian signals reduces to linear Wiener filtering (Bouchet, Gispert & Puget 1996; Tegmark & Efstathiou 1996).

## 2 SIMULATED MAP OBSERVATIONS

The simulated input components used here are identical to those described in HJLB98, so that a direct comparison between the MAP and Planck Surveyor results can be made. These simulations were performed by Gispert & Bouchet (1997) and consist of a  $10^\circ \times 10^\circ$  field for each of the six foreground components described above. The realisations of the input components used are shown in Figure 1. Each component is plotted at  $50 \text{ GHz}$  and, for illustration purposes, has been convolved with a Gaussian beam of FWHM equal to  $12.6$  arcmin, which is the highest resolution of the current design for the MAP satellite. For convenience, the mean of each map is set to zero, in order to highlight the relative level of fluctuations due to each component.

The primary CMB fluctuations are a realisation of COBE-normalised standard  $\Lambda$ CDM with critical density and  $H_0 = 50 \text{ km s}^{-1} \text{ Mpc}^{-1}$ . IRAS  $100\text{-}\mu\text{m}$  maps are used as spatial templates for the

arXiv:astro-ph/9810236v1 15 Oct 1998

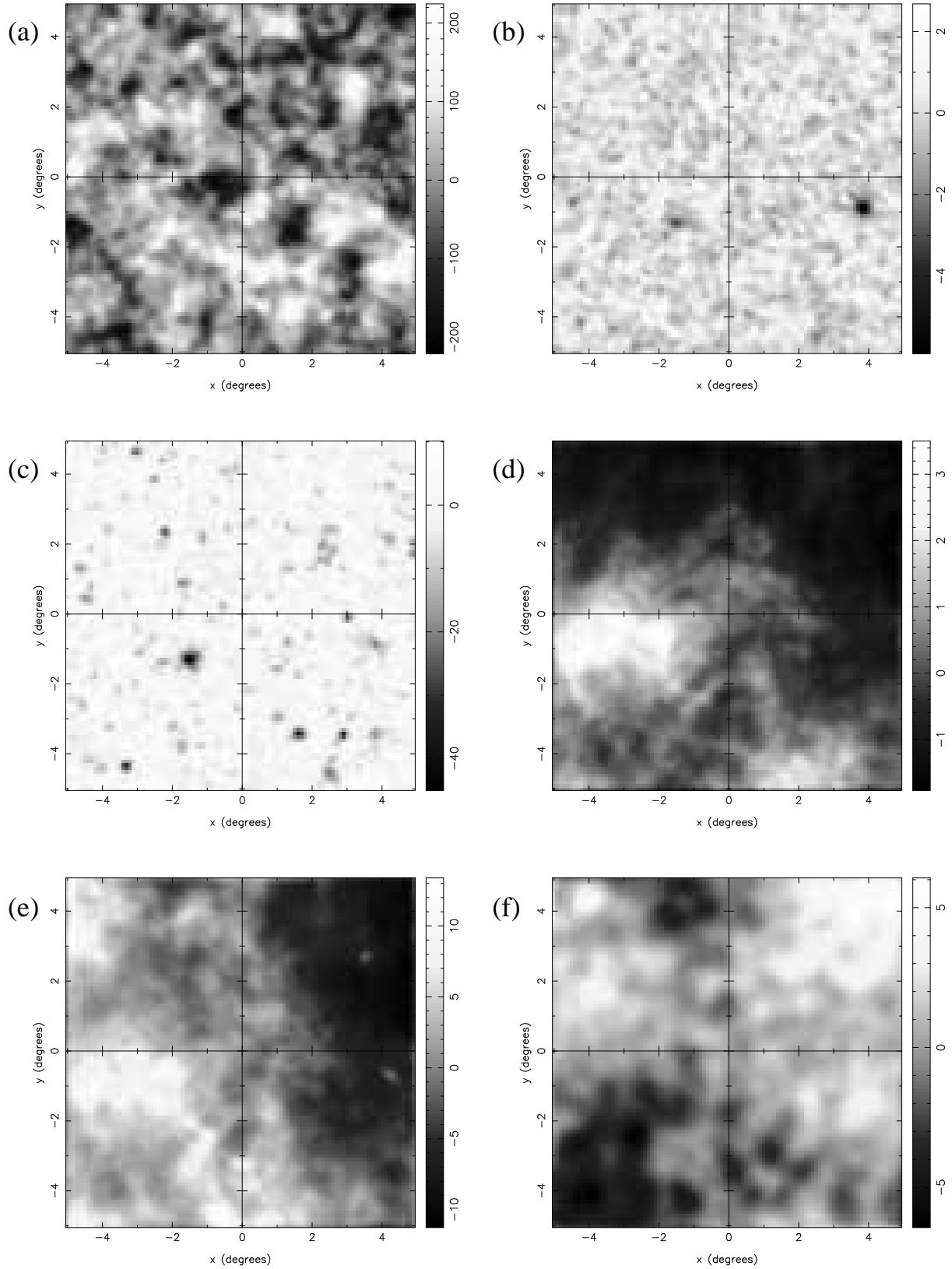


**Figure 1.** The  $10^\circ \times 10^\circ$  realisations of the six input components used to make simulated MAP observations: (a) primary CMBR fluctuations; (b) kinetic SZ effect; (c) thermal SZ effect; (d) Galactic dust; (e) Galactic free-free; (f) Galactic synchrotron emission. Each component is plotted at 50 GHz and has been convolved with a Gaussian beam of FWHM equal to 12.6 arcmin, the maximum angular resolution proposed for the MAP satellite. The map units are equivalent thermodynamic temperature in  $\mu\text{K}$ .

**Table 1.** Proposed observational parameters for the MAP satellite. Angular resolution is quoted as FWHM for a Gaussian beam. Sensitivities are quoted for 12 months of observations.

|   |     |     |     |     |      |
|---|-----|-----|-----|-----|------|
| Central frequency (GHz):                              | 22  | 30  | 40  | 60  | 90   |
| Fractional bandwidth ( $\Delta\nu/\nu$ ):             | 0.2 | 0.2 | 0.2 | 0.2 | 0.2  |
| Transmission:   | 1.0 | 1.0 | 1.0 | 1.0 | 1.0  |
| Angular resolution (arcmin):                          | 56  | 41  | 28  | 21  | 12.6 |
| $\Delta T$ sensitivity ( $\mu\text{K}$ ) (17' pixel): | 26. | 32. | 27. | 35. | 35.  |

dust and free-free components; the correlated emission from these two components is described by HJLB98. Haslam 408 MHz maps (Haslam et al. 1982) are used as the spatial template for the synchrotron emission to which was added Gaussian small scale structure following a  $C_\ell \propto \ell^{-3}$  power law on angular scales below 0.85 degrees. The kinetic and thermal SZ effects are generated using a Press-Schechter formalism, as discussed in Bouchet et al. (1997) and a King model for the cluster profiles. The MAP satellite is not designed to be sensitive to either of the SZ effects but they are included here for completeness.

Using the realisations for each physical component and the design specifications summarised in Table 2, it is straightforward to simulate MAP satellite observations. The simulated observations are produced by integrating the emission due to each physical component across each waveband, assuming the transmission is uniform across the band. At each observing frequency, the total sky emission is convolved with a beam of the appropriate FWHM. Finally, isotropic noise is added to the maps, assuming a spatial sampling rate of FWHM/2.4 at each frequency. We have assumed that any striping due to the scanning strategy and  $1/f$  noise has been removed to sufficient accuracy that any residuals become negligible.

Figure 2 shows the rms temperature fluctuations as a function of observing frequency due to each physical component, after convolution with the beam. The rms noise per pixel at each frequency is also plotted (this noise is calculated for one year of observations and is based upon the current design of the satellite as reported in the MAP NASA home page). We see from the figure that, as expected, the rms temperature fluctuation of the CMB is almost constant across the frequency channels, the only variations being due to the convolution with beams of different sizes. Furthermore, it is seen that the CMB is consistently above the noise level, but only at the very lowest frequency do any of the other physical components become significant. At 22 GHz it is seen that the free-free and synchrotron components just reach above the noise level but are still well below the level of the CMB. This is to be expected since the MAP satellite is designed not to make separate maps of the individual components, but only to provide sufficient information about the foreground emission in order to perform an accurate subtraction from the CMB. This should be contrasted with the Planck Surveyor mission (Bersanelli et al. 1996), which is designed to produce all-sky maps of the foreground components as well as the CMB.

The observed maps at each of the five MAP frequencies are shown in Figure 3 in units of equivalent thermodynamic temperature measured in  $\mu\text{K}$ . The coarse pixelisation at the lower observing frequencies is due to the FWHM/2.4 sampling rate. Moreover, at these lower frequencies the effect of convolution with the relatively large beam is also easily seen. It is also seen that, as expected, the CMB emission dominates each of the frequency channels.

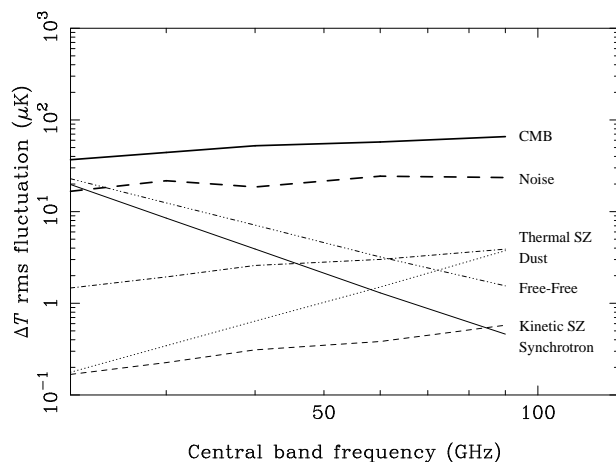


**Figure 2.** The rms thermodynamic temperature fluctuations at the MAP satellite observing frequencies due to each physical component, after convolution with the appropriate beam and using a sampling rate of FWHM/2.4. The rms noise per pixel at each frequency channel is also plotted.

### 3 THE COMPONENT SEPARATION

The component separation is performed using the Fourier space MEM algorithm developed by HJLB98, and the reader is referred to that paper for details of the method. In the absence of non-Gaussian signals the method reduces to linear Wiener filtering. In this Section, we apply the MEM algorithm to the simulated MAP data discussed in Section 2. Since the dominant contributions to the MAP data are the CMB and the pixel noise, which are both Gaussian, the results of the MEM algorithm should be very similar to those obtained using a Wiener filter approach (Bouchet, Gispert & Puget 1996; Tegmark & Efstathiou 1996). Our primary aim is simply to determine the accuracy to which the CMB emission can be recovered from MAP observations after such a component separation has been performed.

As discussed in HJLB98 there are several layers of information that we can use in the analysis of the data. For the CMB and SZ effects the frequency spectra is accurately known. For the Galactic emissions this is not true. However, as discussed in Jones et al. (1998b) it is possible to use the data itself to constrain the spectral dependence of any Galactic emission that is significant in the data. If it is not a significant component then the uncertainty in the spectral index will only affect the reconstruction of that Galactic component and not the reconstruction of any of the other components. Therefore, in this letter, we assume perfect knowledge of the frequency spectra of each component.

Our other prior knowledge concerns the spatial distribution, or power spectrum of the various emission components. We are never entirely ignorant of the shape of the power spectra for the foregrounds in the data. In HJLB98 two levels of power spectrum information were used. The first assumed no information on the power spectra of any component and the second assumed perfect knowledge of the power spectra and cross-correlation information. In this letter we will assume a more conservative approach than the latter but also remembering that we have some prior information on the components. We choose to use the best guess theoretical power spectrum for each component. This is a white noise power spectra for the two SZ effects, standard CDM for the CMB and an  $\ell^{-3}$  power spectra for the Galactic components. In any case, as noted in HJLB98, the MEM algorithm is an iterative process and

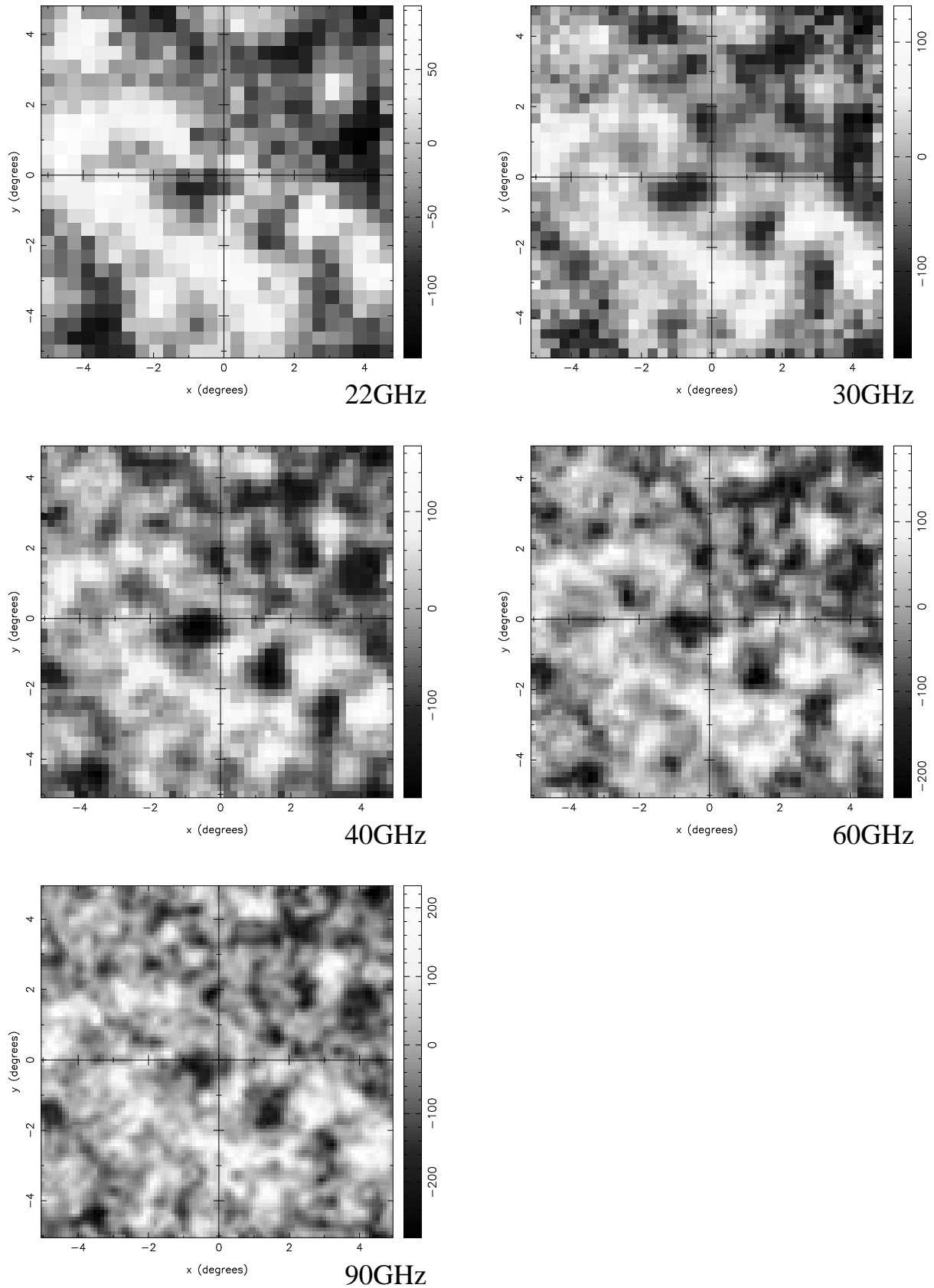


**Figure 3.** The  $10^\circ \times 10^\circ$  maps observed at each of the five MAP frequencies listed in Table 2. At each frequency we assume a Gaussian beam with the appropriate FWHM and a sampling rate of FWHM/2.4. Isotropic noise with the relevant rms has been added to each map. The map units are equivalent thermodynamic temperature in  $\mu\text{K}$ .

the initial guess for the power spectra does not greatly affect the final reconstructions.

### 3.1 The reconstructed CMB map

The reconstruction of the CMB component is shown in Figure 4. The greyscale in this figure was chosen to coincide with that of Fig. 1 in order to enable a more straightforward comparison with the true map. At least by eye the CMB has been reproduced quite accurately. The reconstructions of the other physical components are significantly worse and are not plotted. In fact, the only other components for which the reconstruction differs significantly from zero are the free-free and synchrotron Galactic components. This is expected as the other three components are well below the noise (see Figure 2) in all frequency channels. The free-free and synchrotron reconstructions appear smoothed to a larger degree than the CMB reconstruction which is also expected because the two Galactic components only appear above the noise in the lowest resolution (22 GHz) channel. Further tests on the thermal SZ effect show that only clusters with an integrated decrement of  $> 250\mu\text{K}$  (at 22 GHz) will be observable with the MAP satellite and even then the reconstructed decrement is severely underestimated. This is because the frequency dependence of the thermal SZ at frequencies below 100 GHz closely follows that of the CMB and it is very difficult to extract the information on the SZ effect from the data.

In order to obtain a quantitative description of the accuracy of the reconstructions, we calculate the rms of the residuals. For any particular physical component, this is given by

$$e_{\text{rms}} = \left[ \frac{1}{N} \sum_{i=1}^N (T_i^{\text{rec}} - T_i^{\text{true}})^2 \right]^{1/2} \quad (1)$$

where  $T_i^{\text{rec}}$  and  $T_i^{\text{true}}$  are respectively the reconstructed and true temperatures in the  $i$ th pixel and  $N$  is the total number of pixels in the map. The value of  $e_{\text{rms}}$  for the CMB reconstruction is  $22\mu\text{K}$  per  $12.6'$  pixel. We note that this is very close to the desired  $20\mu\text{K}$  accuracy generally quoted for the MAP satellite. This error should be contrasted with the result obtained by using the 90 GHz data channel as the CMB map. In this case, the error on the map is  $46\mu\text{K}$  (of which  $45\mu\text{K}$  is due to instrumental noise and  $10\mu\text{K}$  is due to the presence of the unsubtracted foregrounds), so some form of component separation is clearly desirable.

As mentioned above, the other physical components were only poorly reconstructed. Indeed no recovery of the dust or either SZ effect was possible at all, and only a low-resolution reconstructions of the other two components were obtained. The rms errors on the free-free and synchrotron reconstructions were  $0.6\mu\text{K}$  and  $0.07\mu\text{K}$  respectively. By comparing these rms errors with the peak amplitudes in each map, which are  $1.0\mu\text{K}$  and  $0.10\mu\text{K}$  respectively, we see that the reconstructions are not very accurate.

As a further test of the quality of the CMB reconstruction, we plot the amplitudes of the reconstructed pixel temperatures against those of the true map. The temperature range of the true input map is divided into 100 bins. Three contours are then plotted which correspond to the 68, 95 and 99 per cent points of the distribution of corresponding reconstructed temperatures in each bin. Clearly, a perfect reconstruction would be represented by a single diagonal contour of unit gradient with width equal to the bin size. Figure 5 shows this comparison for the CMB reconstruction from the MAP data. The gradient of the best fit line is 1.03 and the 68 per cent contours lie approximately  $25\mu\text{K}$  on either side of the true value. This agrees with the value for the  $e_{\text{rms}}$  quoted above. Figure 6 shows the

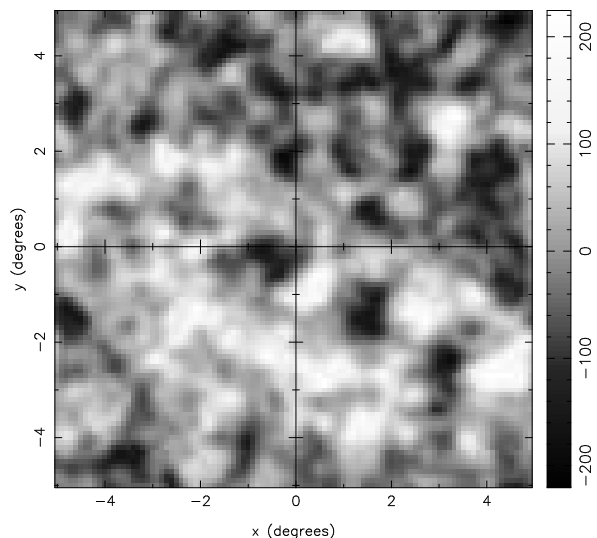


**Figure 4.** MEM reconstruction of the  $10^\circ \times 10^\circ$  CMB map shown in Fig. 1, using the theoretical power spectra information (see text). The map is plotted at 50 GHz and has been convolved with a Gaussian beam of FWHM equal to  $12.6$  arcmin. The map units are equivalent thermodynamic temperature in  $\mu\text{K}$ .

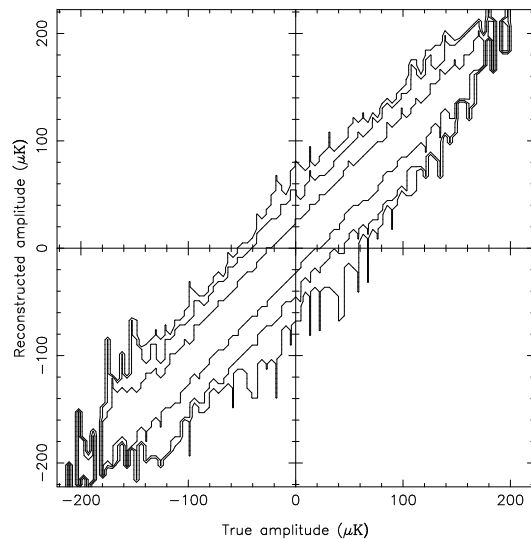


**Figure 5.** Comparison of the CMB true map with the reconstructed map using the MEM algorithm. The horizontal axes show the true map amplitude within a pixel and the vertical axes show the reconstructed amplitude. The contours contain 68, 95 and 99 per cent of the pixels respectively.

same comparison for the case in which the highest frequency data channel as used as the CMB reconstruction at  $12.6'$  resolution. We see that in this case the 68 per cent contour is much wider, corresponding to about  $45\mu\text{K}$  errors, in agreement with the  $e_{\text{rms}}$  value quoted above.

### 3.2 The reconstructed CMB power spectrum

Since the component separation is performed in the Fourier domain, it is straightforward to compute the reconstructed power spectrum of the CMB component. As noted in HJLB98 it is also straightforward to calculate the errors on the reconstructed power spectrum using the inverse Hessian. Figure 7 shows the power spec-

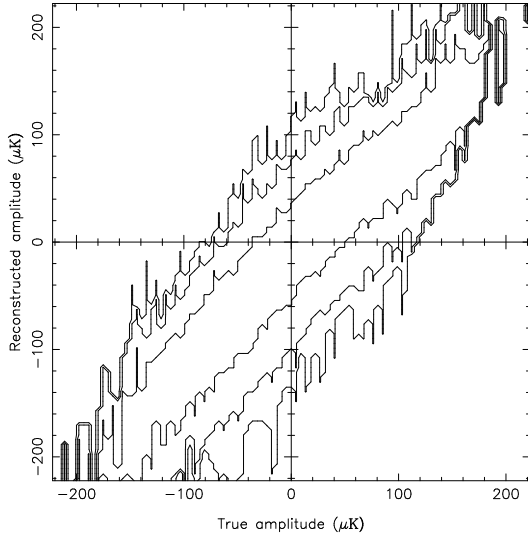


**Figure 6.** As for Figure 5 but using the 90 GHz data channel as the CMB ‘reconstruction’.

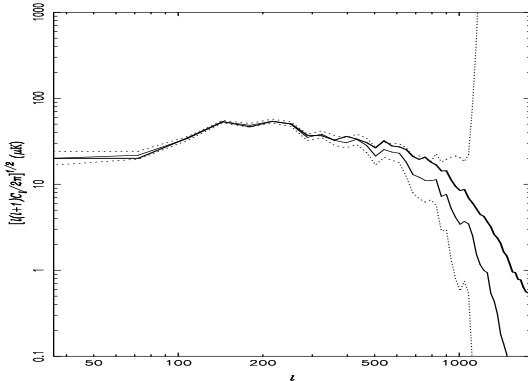


**Figure 7.** Reconstructed power spectrum, in a  $10^\circ \times 10^\circ$  field, for the CMB simulation (bold line) compared to the true power spectrum (faint line). The 68 per cent confidence limits (dotted lines) are also shown.

trum (bold line) of the reconstructed CMB map compared to the power spectrum (faint line) of the input map. The 68 per cent confidence limits on the power spectrum reconstruction are also shown (dotted lines). It is seen that the true power spectrum is almost always contained within the 68 per cent confidence intervals. These confidence limits on the power spectrum are calculated by assuming a Gaussian profile for the posterior probability distribution around its maximum (see HJLB98). We see that the power spectrum of the reconstructed map is reasonably accurate for  $\ell \lesssim 500$ , at which point the reconstructed spectrum begins slightly to underestimate the true value, and beyond  $\ell \approx 1000$  the input power spectrum is severely underestimated. This behaviour is due mainly to the effects of beam convolution and presence of instrumental noise. By using some form of rescaled filter, it is possible to boost the reconstructed power spectrum at high  $\ell$  so that it lies closer to the input spectrum, but only at the cost of increasing the rms error of the corresponding reconstructed CMB map (see HJLB98). Therefore, such a procedure has not been carried out here.

## 4 DISCUSSION AND CONCLUSIONS

In this paper, we have analysed simulated MAP observations in a  $10^\circ \times 10^\circ$  field, in order to separate the CMB emission from various foreground contaminants and determine how accurately the CMB emission can be recovered. The algorithm used to perform the component separation is the Fourier space maximum-entropy method discussed by Hobson et al. (1998), which reduces to a Wiener filter in the absence of non-Gaussian signals. The simulated observations include contributions from primary CMB, kinetic and thermal SZ effects, and Galactic dust, free-free and synchrotron emission. Assuming knowledge of both the one-dimensional ensemble average power spectrum for each component and its frequency behaviour, we find that the CMB emission can be reconstructed with an rms accuracy of  $22\mu\text{K}$  per 12.6 arcmin pixel. We note that this represents a substantial improvement as compared to the individual temperature sensitivities of the raw data channels, and thus indicates that some form of component separation is desirable for MAP observations. We also find that the power spectrum of the reconstructed CMB map lies close to the true power spectrum for  $\ell \lesssim 1000$ . In contrast to our analysis of simulated Planck Surveyor observations (Hobson et al. 1998), we find that it is not possible to recover the emission from Galactic dust or the kinetic/thermal Sunyaev-Zel’dovich effects, although low-resolution reconstructions of the Galactic free-free and synchrotron emission were obtained.

We have also repeated the component separation using a straightforward Wiener filter algorithm, and find that, as expected, the reconstructions are very similar to those presented above and the rms error on the reconstructed CMB map is almost identical. Moreover, both techniques take the same computational time as they are based upon similar calculations in Fourier space. As mentioned above, the similarity of the results is due to the fact that the dominant contributions to the MAP data are the CMB and instrumental noise, which are both Gaussian. Thus, although several non-Gaussian foregrounds were included in the simulated observations, the angular resolution and frequency coverage of the MAP satellite preclude the presence of significant non-Gaussian effects in the data (although this is certainly not the case for the Planck Surveyor satellite). If, however, the input CMB component in the MAP simulations is replaced by a realisation of CMB fluctuations due to cosmic strings, there still exists a significant non-Gaussian signal in the data. In this case we find that the rms error on the CMB reconstruction is consistently  $2\mu\text{K}$  lower for the MEM algorithm as compared to the Wiener filter.

## ACKNOWLEDGEMENTS

AWJ acknowledges King’s College, Cambridge, for support in the form of a Research Fellowship. We would like to thank Francois Bouchet and Richard Gispert for kindly providing the simulations used in this paper.

## REFERENCES

- Bouchet F.R., Gispert R., Boulanger F., Puget J.L., 1997, in Bouchet F.R., Gispert R., Guideroni B., Tran Thanh Van J., eds, Proc. 36th Moriond Astrophysics Meeting, Microwave Anisotropies. Editions Frontière, Gif-sur-Yvette, p. 481
- Bouchet F.R., Gispert R., Puget J.L., 1996, in Dwek E., ed., Proc. AIP Conf. 348, The mm/sub-mm foregrounds and future CMB space missions. AIP Press, New York, p. 255

- Gispert R., Bouchet F.R., 1997, in Bouchet F.R., Gispert R., Guideroni B., Tran Thanh Van J., eds, Proc. 16th Moriond Astrophysics Meeting, Microwave Anisotropies. Editions Frontière, Gif-sur-Yvette, p. 503
- Haslam C. G. T et al., 1982, A&AS, 47, 1
- Hobson M.P., Jones A.W., Lasenby, A.N., Bouchet, F.R., 1998a, MNRAS, in press
- Hobson M.P., Barreiro R.B., Toffalati L., Lasenby A.N., Sanz J.L., Jones A.W., Bouchet F.R., 1998b, MNRAS, submitted
- Jones A. W., Hancock S., Lasenby A. N., Davies R. D., Gutiérrez C. M., Rocha G., Watson R. A., Rebolo R., 1998a, MNRAS, 294, 582
- Jones A. W., Hobson, M.P., Mukherjee, P., Lasenby A.N., 1998b, to appear in Proc. of 'The CMB and the Planck Mission', Santander
- Maisinger K., Hobson M.P., Lasenby A.N., 1997, MNRAS, 290, 313
- Tegmark M., Efstathiou G., 1996, MNRAS, 281, 1297
- Toffalati L., Argüeso Gómez F., De Zotti G., Mazzei P., Francheschini A., Danese L., Burigana C., 1998, MNRAS, 297, 117

This paper has been produced using the Royal Astronomical Society/Blackwell Science  $\LaTeX$  style file.